Accurate Capacitive Current Balancing in Multistring LED Lighting Systems Based on Switched-Capacitor-Controlled LCC Resonant Network

C. S. Wong, *Student Member, IEEE*, K. H. Loo, *Member, IEEE*, Y. M. Lai, *Senior Member, IEEE*, Martin H. L. Chow, *Member, IEEE*, and Chi K. Tse, *Fellow, IEEE*

***Abstract*—The combination of high-frequency ac drive and capacitors offers an attractive passive current balancing solution for multistring light-emitting diodes (LED) lighting systems due to the advantages of compactness, high efficiency, and ease of modularity. Given that frequency-controlled resonant converters are commonly used as high-frequency ac drivers, the conventionally used switching frequency modulation could impair the effectiveness of capacitive balancing as the impedance of the balancing capacitors is a sensitive function of the switching frequency which is constantly varied for the purpose of output voltage regulation. In this paper, a constant-frequency capacitive impedance current balancing method is proposed. Compared to the conventional method, output voltage regulation of resonant converter is achieved by modulating the resonant frequency of resonant tank by switch-controlled capacitor (SCC) technique, which gives rise to constant balancing capacitor's impedance and constant LED current over a wide range of load conditions. Its implementation in an LCC resonant network is studied in this paper and a systematic design procedure of a SCC-based constant-frequency LCC resonant converter is presented. The effectiveness of the proposed method is experimentally verified by a 70-W experimental prototype.**

***Index Terms*—Current balancing, capacitive impedance balance, *LCC* resonant network, multi-LED strings, switch-controlled capacitor (SCC).**

I. Introduction

With the advantageous features offered by light-emitting diodes (LEDs), such as high efficiency and long life span, there is an increasing use of LEDs in many high-luminance lighting applications such as street lighting, traffic signalling, and general lighting [1]. In order to obtain a sufficient level of light output for these applications, a large number of LEDs are typically used. A bulky series connection of LEDs represents a simple solution, yet it gives rise to the safety concern that a high-voltage stress is imposed on the LED driver. Thus, several LED strings are used collectively and driven in parallel by a common bus voltage [2]. However, due to the manufacturing spreads of the $I-V$ characteristics and the negative temperature coefficient of LEDs, current tends to distribute nonuniformly among the parallel-connected LED strings, which leads to nonuniform light output or even a rapid deterioration of LEDs [3]. As a result, additional mechanism must be provided by the LED driver to equalize the currents among the multiple LED strings.

Recently, current balancing techniques have been discussed extensively in the literature and generally they can be categorized into active and passive methods. For active balancing methods, linear-mode or switch-mode current regulators are used to regulate and balance the current in each LED string, such that an accurate current sharing can be achieved, but significant power loss in linear regulators, high control complexity or high implementation cost associated with switch-mode regulators are their distinct disadvantages, which make them unsuitable for high-power applications [3]–[8]. In view of the drawbacks of active balancing methods, significant research efforts have been directed towards passive balancing methods utilizing lossless and reactive components, such as capacitors and inductors, in conjunction with the use of high-frequency ac voltage or current sources [9]–[20]. To enable the flow of the ac current, bidirectional current path must be made available which is usually accomplished by connecting a bridge rectifier before an LED string or connecting two LED strings in an antiparallel structure. For inductive balancing, 1:1 coupled inductors or transformers are typically employed [9]–[11]. By the property of flux balance, the currents of the two LED strings that are connected to the two windings of a coupled inductor are automatically balanced through the connection shown in Fig. 1. However, when more pairs of LED strings are involved, a large number of coupled inductors are needed, which, as a result, poses challenges to the ease of modularity as well as increases the size and cost of the LED driver dramatically. Furthermore, the efficiency of the LED driver is penalized due to increased conduction and core losses.

In contrast to inductive balancing, a more efficient capacitive balancing is introduced as an alternative passive balancing method. This method can be further divided into capacitive charge balance [12], [15], [18]–[20] and capacitive impedance

Manuscript received December 4, 2015; revised March 15, 2016; accepted April 26, 2016. Date of publication May 6, 2016; date of current version December 9, 2016. This work was supported by in part by the University Grants Committee of the Hong Kong Special Administrative Region, Research Grants Council under Theme-Based Research Project T22-715/12-N, and in part by PolyU's Internal Competitive Research under Grants PolyU 5177/13E and PolyU 152191/15E. Recommended for publication by Associate Editor M. Ponce-Silva.

The authors are with the Department of Electronic and Information Engineering, The Hong Kong Polytechnic University, Hung Hom, Hong Kong (e-mail: chi.shing.wong@connect.polyu.hk; kh.loo@polyu.edu.hk; enymlai@polyu.edu.hk; martin.chow@polyu.edu.hk; michael.tse@polyu.edu.hk).

Color versions of one or more of the figures in this paper are available online at http://ieeexplore.ieee.org.

Digital Object Identifier 10.1109/TPEL.2016.2564441

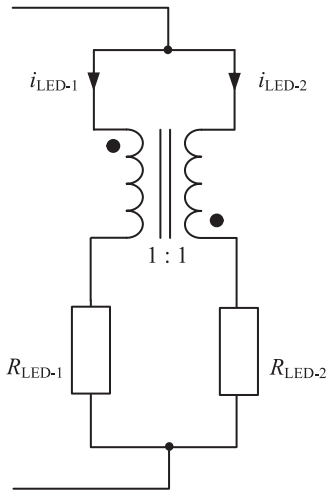

Fig. 1. Inductive current balancing.

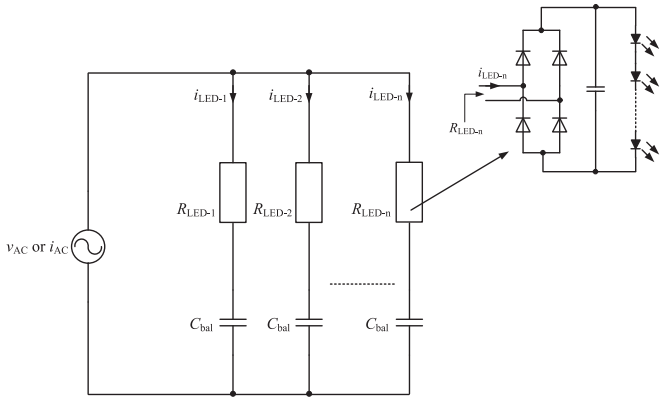

Fig. 2. Capacitive impedance current balancing.

balance [13], [14], [16], [17]. Similar to inductive balancing, capacitive charge balance can only be achieved in pairs of LED strings, hence the total number of LED strings is restricted to even number. When the number of LED strings is arbitrary, capacitive impedance balance or the hybridization of the two are used. For capacitive impedance balance, a high-frequency ac voltage/current source is used to drive serially connected balancing capacitors and LED strings, as shown in Fig. 2. The impedance of the balancing capacitors is deliberately designed to be much larger than the ac equivalent resistance of the LED strings so that the LED current is governed by the impedance of the balancing capacitors, and hence rendered insensitive to the variations of LED properties.

From the discussion above, one can find that capacitive impedance balance enjoys several advantages apart from high efficiency and compactness. First, modular design can be easily realized by connecting more identical balancing capacitors and LED strings to the common ac source. In addition, the high-frequency ac source can be readily obtained from well-known inverter topologies such as resonant converters. However, multistring LED lighting systems commonly suffer from the disconnection of LED strings due to malfunctioning and the need to compensate for this disruption and ensure the continuous operation of lighting systems. For this purpose, short-circuit protection is inherent in capacitive impedance balance due to the current-limiting function provided by the capacitive impedance. Open-circuit protection, on the other hand, requires more careful design and will be discussed later in this paper.

In general, special cautions should be taken when current-source LED drivers are used. In [2], a protective circuit is included so that the circuit will be immediately shut down under abnormal load conditions. Although the proposed method can prevent other normal LED strings from being damaged, it cannot ensure continuous operation after load failures. Therefore, it only finds limited applications such as in backlight systems. In a more recent attempt in [17], the authors combine inductive balance and capacitive impedance balance to ensure an accurate current sharing among multiple LED strings. Although the proposed circuit can withstand any number of string failures and ensure continuous operation, it requires additional circuitries to detect and isolate the damaged strings. In [16], additional protection is necessary for each LED string to maintain a current path in case of any LED becoming open, which increases the cost and complexity of LED drivers as the number of LED strings increases.

On the contrary, the use of capacitive impedance balance alongside with a common ac voltage source provides a simpler solution to isolate the damaged strings and to ensure continuous operation, particularly when LED strings become open [13], [14]. Since the branch impedance is dominated by the impedance of balancing capacitor, the LED current in each string is naturally limited. On the other hand, open-circuit protection can be guaranteed without additional components as the string voltage is clamped by the regulated common bus voltage. Resonant converters are commonly used to generate high-frequency ac voltage alongside with switching frequency modulation. The main drawback of this approach is that since the impedance of the balancing capacitors is a function of switching frequency, the LED current in each string varies as new switching frequency is applied when LED drivers respond to load failures or input voltage variations. In other words, the effect of damaged LEDs cannot be isolated from the healthy LEDs although circuit operation remains uninterrupted. The result of reduced series impedance with increasing switching frequency can cause an increase in current stress or accelerated degradation of the healthy LEDs.

In this paper, a constant-frequency capacitive current balancing method for multistring LED lighting systems is proposed. The proposed method achieves output voltage regulation by modulating the resonant frequency of resonant converter by means of switch-controlled capacitor (SCC) technique. By fixing switching frequency, the impedances of balancing capacitors are kept constant under any load conditions and the effect of damaged LEDs is isolated and cannot be transferred to the healthy LEDs. The paper will focus on the discussion and analysis of LCC resonant network but the general idea can be extended to other resonant networks. In Section II, the drawback of employing switching frequency modulation in the presence of capacitive current balancing will be discussed in detail and

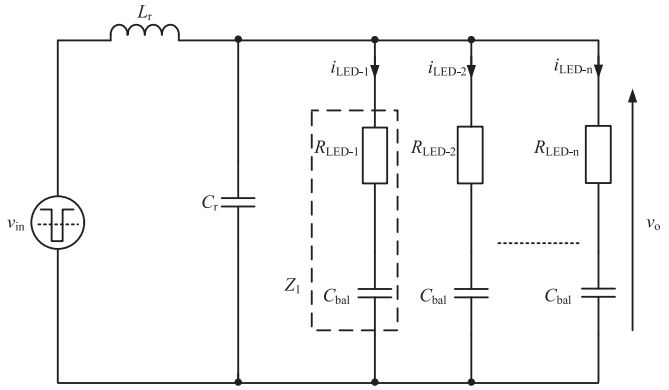

Fig. 3. Example of LCC resonant network used for capacitive impedance current balancing.

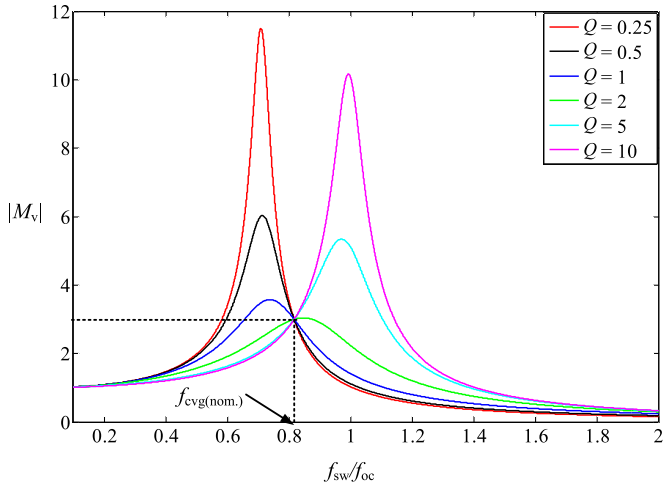

Fig. 4. Frequency responses of LCC resonant network for different values of Q with the number of LED branches being unchanged, where Q is the loaded quality factor as defined in [14].

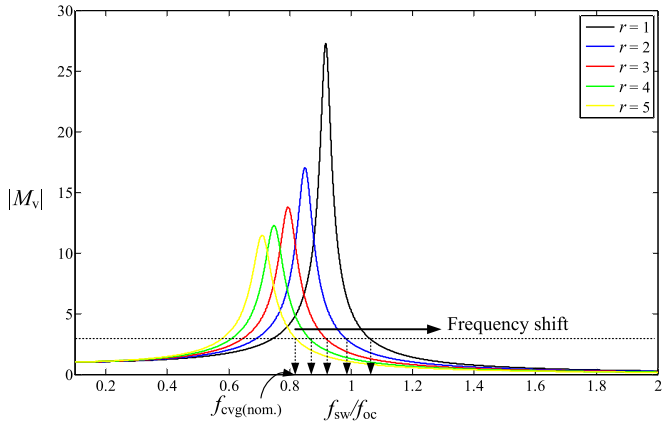

Fig. 5. Frequency responses of LCC resonant network for different number of LED strings opened, where r is the number of conducting LED strings.

simulation results are presented for illustration. In Section III-A, the principle of the proposed current balancing method will be discussed. In Sections III-B and III-C, the working principle of SCC and its control design in the context of LCC resonant converter will be presented, followed by discussion of a design example in Section III-D. Finally, the designed example will be experimentally verified in Section IV.

II. Issue of Conventional Regulation Method in LCC Resonant Network

Fig. 3 shows an example of LCC resonant network excited by a bipolar square voltage. This driver architecture and its mathematical expressions were analyzed in detail in [14] and will not be repeated here. The resonant network consists of a resonant inductor L_r, resonant capacitor C_r, and branch impedances Z_n (i.e., $R_{\text{LED}-n} + 1/j\omega C_{\text{bal}}$) which are composed of identical balancing capacitors C_{bal} and ac equivalent resistances of LED strings $R_{\text{LED}-n}$, where subscript n is the LED string number. All Z_n is dominated by the impedance of the balancing capacitor and driven by the same ac bus voltage v_o, such that the current of each branch is equal and determined by (1). Regulation of LED current can be achieved indirectly by regulating the peak of v_o. As revealed in [14] and shown in Fig. 4, there exists a favorable operating frequency $f_{\text{cvg(nom.)}}$ under which the voltage gain M_v of the resonant network is constant for any values of $R_{\text{LED}-n}$ with the number of LED branches kept constant, and thus a tight output regulation can be achieved. However, this property is not applicable to the extreme cases, especially when one or more LED strings become open. As the strings open, the operating point of the resonant network will shift from the favorable operating condition (i.e., $f_{\text{cvg(nom.)}}$) towards higher frequency. Fig. 5 plots the frequency responses of the LCC resonant network derived in [14] with different number of LED strings opened, where r is the number of conducting LED strings, from which it can be seen that the switching frequency must be increased in order to regulate v_o and this is accompanied by an increase of LED current due to reduced balancing capacitor's impedance. Fig. 6 shows the simulation results for a frequency-modulated LED driver with its specifications listed in Table I. From the simulation results, it can be seen that the average LED current of a normal LED string increases gradually with increasing number of opened LED strings despite v_o being constant, which matches the analysis of Fig. 5 and expression of (1). In the worst case, there exists 34% deviation from the nominal LED current when only one string is conducting. Therefore, in order to avoid a large deviation in LED current, which could affect the luminance output and also increase the current stress on the remaining LEDs, an alternative regulation method in lieu of frequency modulation must be devised such that both the common bus voltage and the balancing capacitive impedance can be kept constant under varying load conditions

$$i_{\text{LED}-n} = \frac{v_o}{Z_n} = \frac{v_o}{\sqrt{R_{\text{LED}-n}^2 + \left(\frac{1}{\omega C_{\text{bal}}}\right)^2}} \tag{1}$$

$$i_{\text{LED}-1} = i_{\text{LED}-2} = i_{\text{LED}-n} \approx v_o \cdot \omega C_{\text{bal}}$$

where $\omega = 2\pi f_{\text{sw}}$.

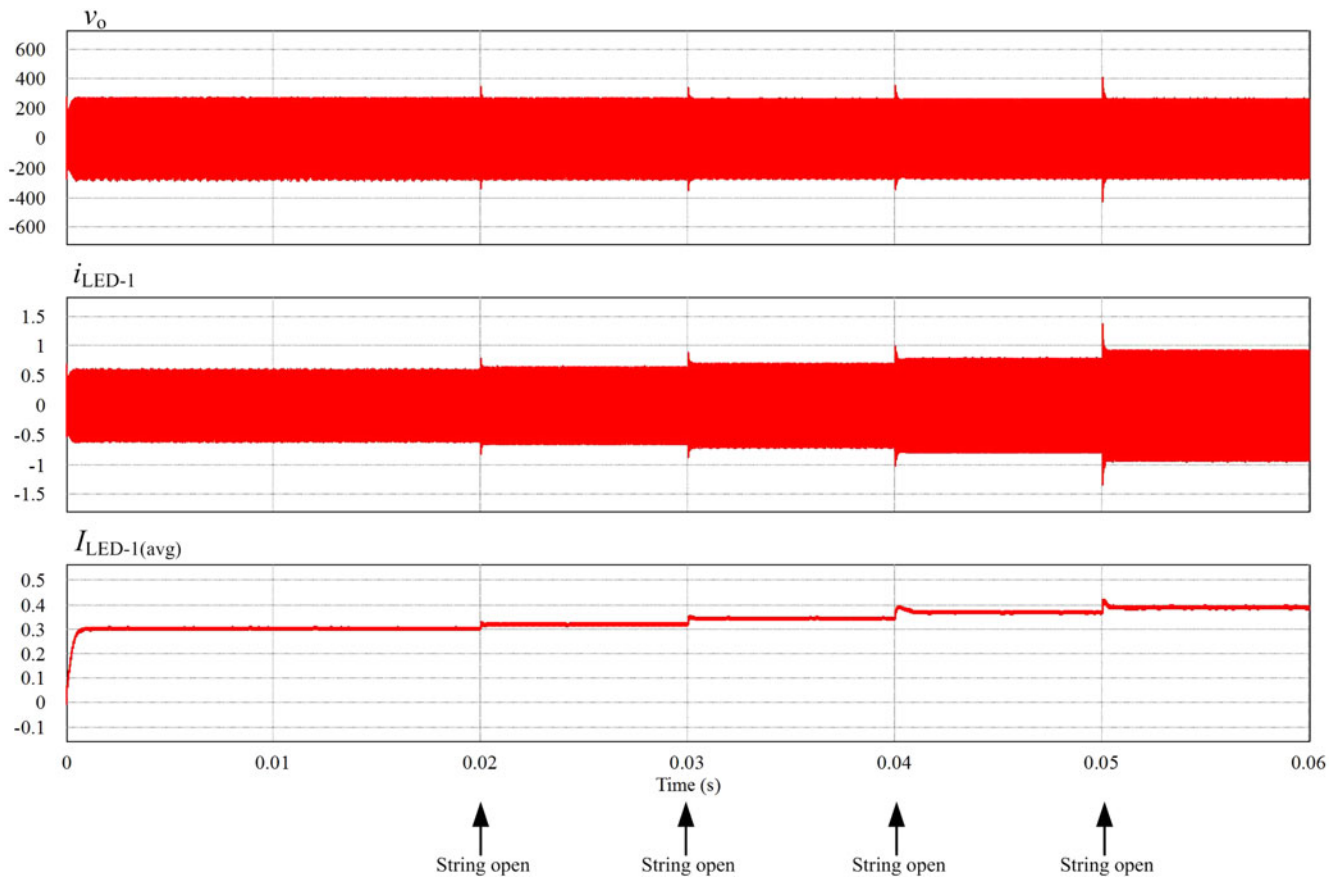

Fig. 6. Simulation results of the LCC resonant network using the conventional regulation method.

TABLE I
SIMULATION SPECIFICATIONS

rms of v_o	168-V
Nominal switching frequency	87 kHz
C_{bal}	4.4 nF
Impedance of C_{bal}	417 Ω
R_{LED}	120 Ω
rms of LED current	400-mA
Number of LED strings	5

III. Circuit Topology and Control of the Proposed Constant-Frequency LCC Resonant Converter

A. Analysis of the Proposed Constant-Frequency Capacitive Current Balancing Method

In this section, an alternative regulation method is introduced to achieve an accurate capacitive impedance current balancing over a wide range of load conditions. Note that the voltage gain of a resonant network is determined by the ratio of the switching frequency to the resonant frequency of the resonant network. In other words, the regulation of a resonant converter can be accomplished by keeping the switching frequency constant while modulating the resonant frequency of the resonant network by means of electronically tuning the tank's component values [21], [22]. The proposed method is applied to the LCC resonant network discussed in [14] with the resonant capacitor implemented by a SCC. The implementation and control strategy will be explained in detail in the next section.

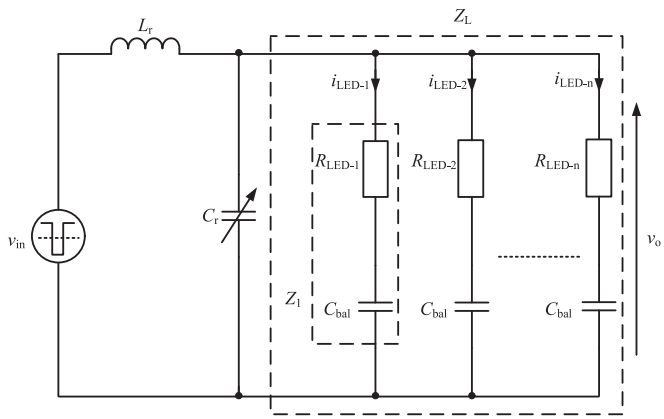

Fig. 7. Modified LCC resonant network with conceptual variable capacitor for mathematical analysis.

Fig. 7 shows the modified LCC resonant network where the conventional fixed resonant capacitor in Fig. 3 is substituted by an electronically tunable capacitor C_r. The total load impedance Z_L and total load current i_o is given by (2) and (3), respectively. To obtain the expression for voltage gain under constant switching frequency, fundamental harmonic approxi-

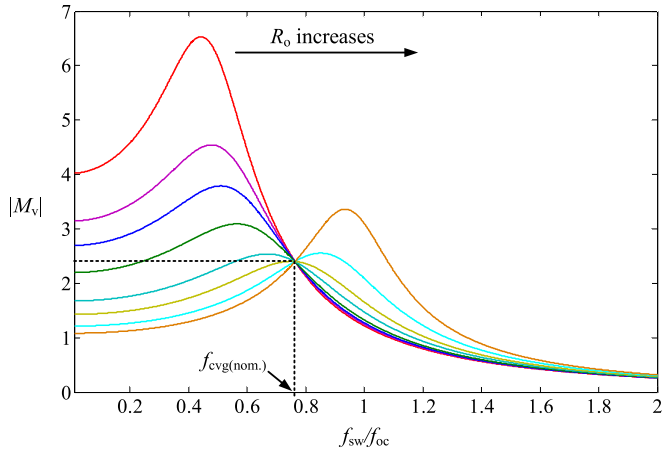

Fig. 8. Frequency responses of the modified LCC resonant network for different values of R_o with the number of LED branches being unchanged.

mation is used here. By voltage division, the voltage gain of the resonant network is given by (5), where $f_{\rm oc}$ is the undamped natural frequency of the resonant tank. As expected, the voltage gain of the resonant tank is related to $f_{\rm oc}$ which can be used as a control parameter for output voltage regulation by varying the effective value of C_r

$$Z_L = Z_1//Z_2//\ldots//Z_n = R_o + \frac{1}{j\omega C_o} \tag{2}$$

where $R_o = \frac{R_{\rm LED}}{n}$ and $C_o = nC_{\rm bal}$.

$$i_o \approx v_o \cdot \omega C_o = \frac{v_o}{X_{\rm C}} \tag{3}$$

where

$$X_C = \frac{1}{2\pi f_{\rm sw} C_o} = kR_o \tag{4}$$

$$M_v = \frac{1 + j2\pi f_{\rm sw} R_o C_o}{\left[1 - \frac{f_{\rm sw}^2}{f_{\rm oc}^2} - (2\pi f_{\rm sw})^2 L_r C_o\right] + j2\pi f_{\rm sw} R_o C_o \left(1 - \frac{f_{\rm sw}^2}{f_{\rm oc}^2}\right)}$$
$$= \frac{1 + \frac{R_o}{X_C}}{\left(1 - \frac{f_{\rm sw}^2}{f_{\rm oc}^2} - \frac{X_L}{X_C}\right) + j\left(\frac{R_o}{X_C}\right)\left(1 - \frac{f_{\rm sw}^2}{f_{\rm oc}^2}\right)} \tag{5}$$

where

$$f_{\rm oc} = \frac{1}{2\pi\sqrt{L_r C_r}} \tag{6}$$

$$X_L = 2\pi f_{\rm sw} L_r. \tag{7}$$

In Fig. 8, the frequency responses of the modified LCC resonant network for various R_o are plotted. The peak voltage gain of the resonant network shifts towards $f_{\rm sw}/f_{\rm oc} = 1$ as R_o increases. In addition, a characteristic frequency $f_{\rm cvg(nom.)}$ exists where the voltage gain is constant for any values of R_o with the number of LED strings kept constant, which makes it an appropriate operating point for achieving good output voltage regulation with different power levels under nominal condition. As a result, by combining this property with the proposed voltage regulation method, an effective load-independent capacitive current balancing is achieved. To determine $f_{\rm cvg(nom.)}$, the magnitude of (5) is differentiated with respect to R_o and the result is set to zero, which gives (8). The associated constant voltage gain can be found by inserting (8) into (5), which gives rise to (9)

$$f_{\rm cvg(nom.)} = \sqrt{1 - \frac{1}{2}\left(\frac{X_L}{X_C}\right)} \tag{8}$$

$$|M_v|_{\rm (cvg)} = \frac{2X_C}{X_L}. \tag{9}$$

By inspecting (5), it can be found that the voltage gain of the resonant network is solely determined by X_L where other variables are known design parameters. The frequency position of the peak voltage gain can then be obtained by differentiating the magnitude of (5) with respect to the normalized frequency $f_{\rm sw}/f_{\rm oc}$ and setting the result to zero, and the result is given by (10). Furthermore, by comparing (10) with (8), it can be found that $f_{\rm cvg(nom.)}$ is always higher than $f_{\rm n(pk)}$ when $X_C >> R_o$. Hence, zero-voltage switching (ZVS) is guaranteed when the operating point is set to $f_{\rm cvg(nom.)}$

$$f_{n(\rm pk)} = \frac{f_{\rm sw}}{f_{\rm oc\ (pk)}} = \sqrt{\frac{1 - \frac{X_L}{X_C} + \left(\frac{R_o}{X_C}\right)^2}{1 + \left(\frac{R_o}{X_C}\right)^2}} \tag{10}$$

$$Z_{\rm in} = jX_L + \left(\frac{1}{j2\pi f_{\rm sw} C_r}//Z_L\right)$$
$$= jX_L + \frac{-jX_L \cdot Z_L\left(\frac{f_{\rm oc}^2}{f_{\rm sw}^2}\right)}{Z_L - jX_L\left(\frac{f_{\rm oc}^2}{f_{\rm sw}^2}\right)} \tag{11}$$

$$Z_{\rm in(cvg)} = jX_L + \frac{-jX_L}{1 - \frac{1}{2}\left(\frac{X_L}{X_C}\right) - j\frac{X_L}{Z_L}}. \tag{12}$$

Besides studying the frequency responses of the resonant network, its input impedance is also examined for determining the circuit rating and circulating power. The expression of input impedance of the LCC resonant network is given by (11) in terms of X_L, Z_L, and $f_{\rm oc}$. Fig. 9 plots the input impedances for different values of X_L with Z_L kept constant. As mentioned, the operating point $f_{\rm cvg(nom.)}$ is always higher than $f_{n(\rm pk)}$ for current balancing and realization of ZVS, which is also equivalent to the inductive impedance region shown in Fig. 9. From Fig. 9, it can be seen that the inductive input impedance of the resonant network decreases with X_L, which implies that X_L cannot be made too small for achieving high efficiency due to the need to reduce circulating power and conduction loss in the resonant network under nominal condition.

On the other hand, the input impedances for different R_o should also be considered. By substituting (8) into (11), the input impedance at $f_{\rm cvg(nom.)}$ can be found and determined by (12). When R_o is made smaller, the input impedance of the resonant network slightly decreases, hence more current is drawn by the resonant network, leading to higher current rating and conduction loss. Nevertheless, the realization of ZVS in

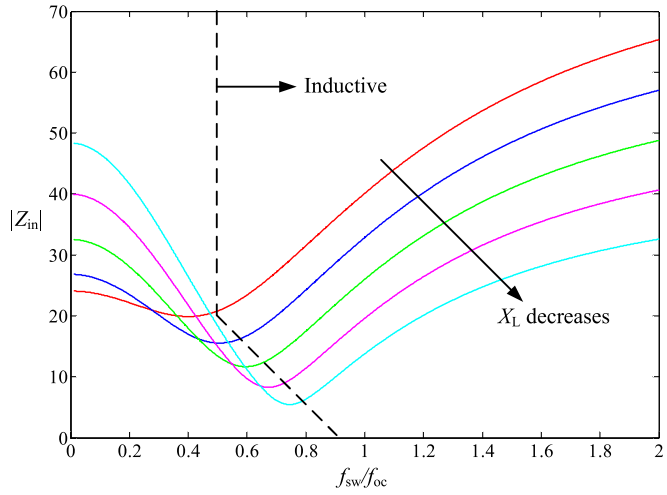

Fig. 9. Input impedances of the modified LCC resonant network for different values of X_L with Z_L being unchanged.

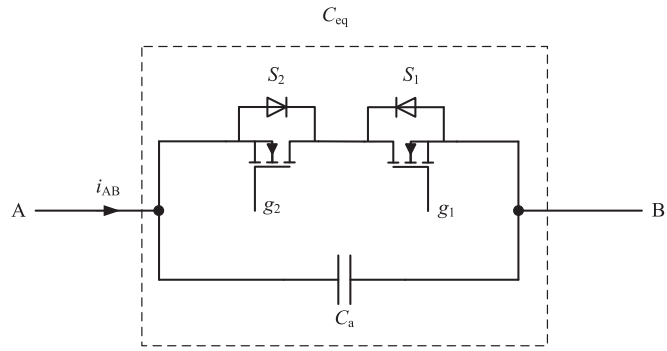

Fig. 10. Schematic diagram of SCC.

SCC under all load conditions can help maintain the driver's efficiency, which will be discussed in the next section.

B. Working Principle of SCC

This section discusses the SCC technique which allows the effective value of the resonant capacitor to be varied electronically so that the output voltage v_o can be regulated by modulating the undamped natural frequency f_{oc} of the resonant tank under constant switching frequency [21], [22]. The schematic diagram of an SCC is shown in Fig. 10 which contains two actively controlled switches (i.e., S_1, S_2) and a fixed capacitor C_a. The key waveforms of the SCC are shown in Fig. 11. Consider that there is a sinusoidal current flowing from A to B, and the two switches are synchronized with the zero-crossing points of the current and turned ON for a fixed control angle α. S_1 is turned ON at the instant when the current passes through zero from negative to positive, and vice versa for S_2. As S_1 is turned ON and the voltage across C_a is zero, the current flows from A to B through S_1 and the body diode of S_2. Upon reaching the control angle α, S_1 is turned OFF and C_a is charged up by i_{AB} until the current direction reverses. Once the current passes through zero from positive to negative, S_2 is turned ON and C_a starts to discharge while the body diode of S_1 remains reverse-biased. When C_a is fully discharged, the current flows from B to A through S_2 and the body diode of S_1 until S_2 is turned OFF again. A similar process occurs for the negative cycle of v_{Ca}. From the analysis above, it can be readily found that v_{Ca} is always zero before the switches are turned OFF, so they are turned OFF at zero voltage inherently. On the other hand, their body diodes are first conducted for the positive/negative current flow before their gate signals are applied, so the switches are also turned ON at zero voltage. As a result, both switches in SCC can be turned ON and OFF with ZVS for any load variation by virtue of its working principle.

By decomposing the waveform of v_{Ca} into harmonic components using Fourier series and considering only the fundamental component, the equivalent resonant capacitance can be derived

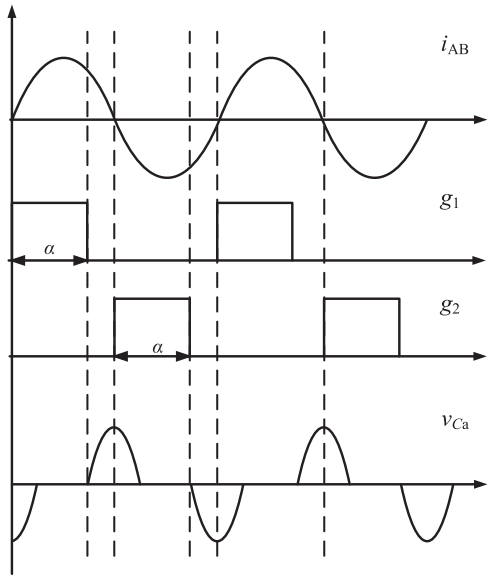

Fig. 11. Waveforms of SCC.

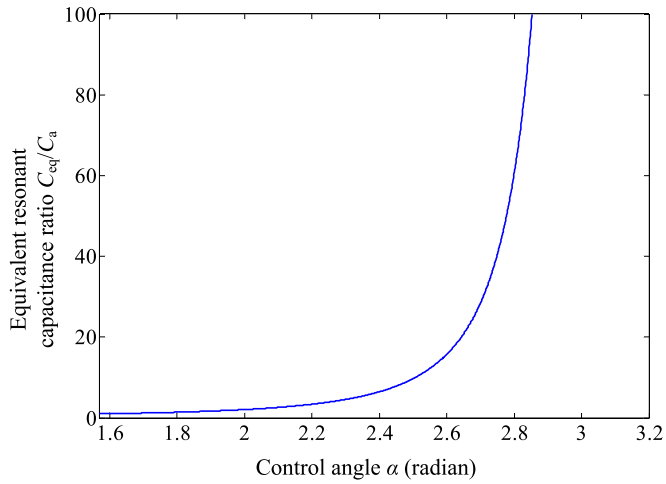

Fig. 12. Ratio of equivalent resonant capacitance C_{eq} to fixed capacitance C_a versus control angle α.

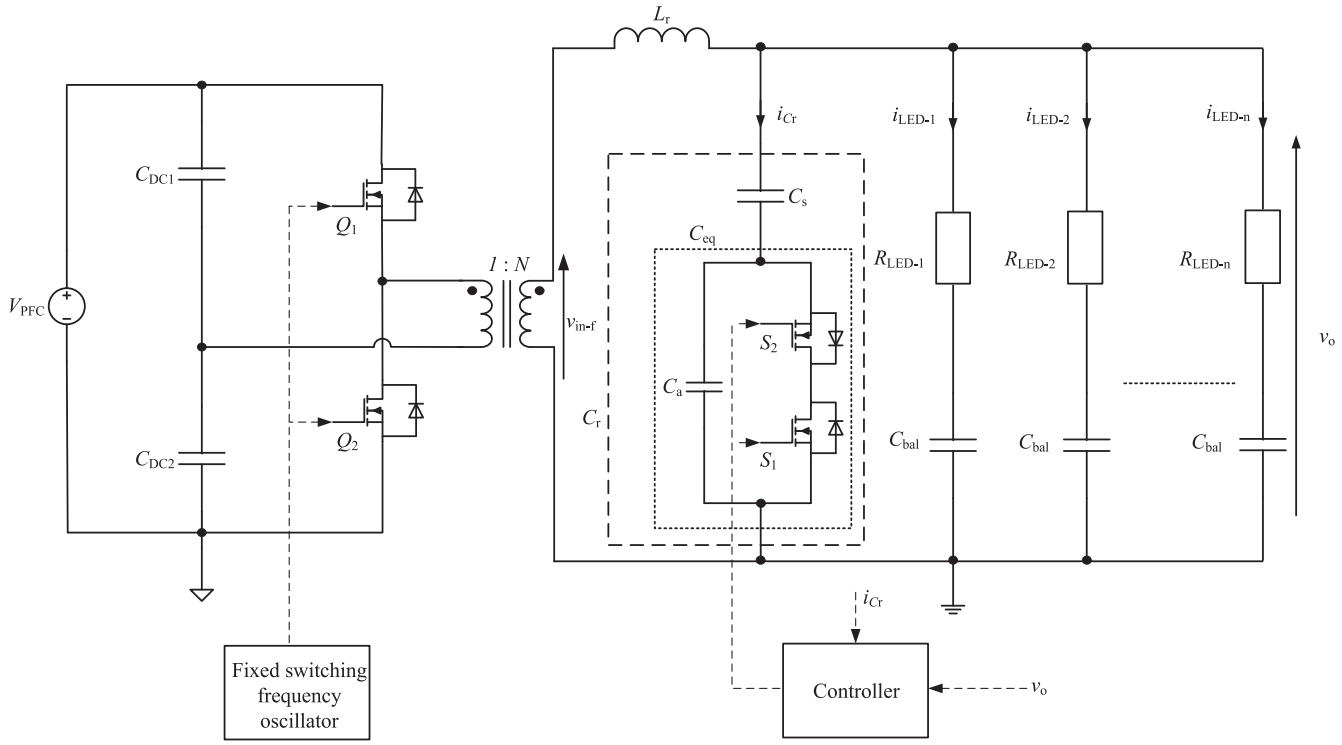

Fig. 13. Schematic diagram of the proposed constant-frequency LCC resonant converter with SCC for capacitive impedance current balancing.

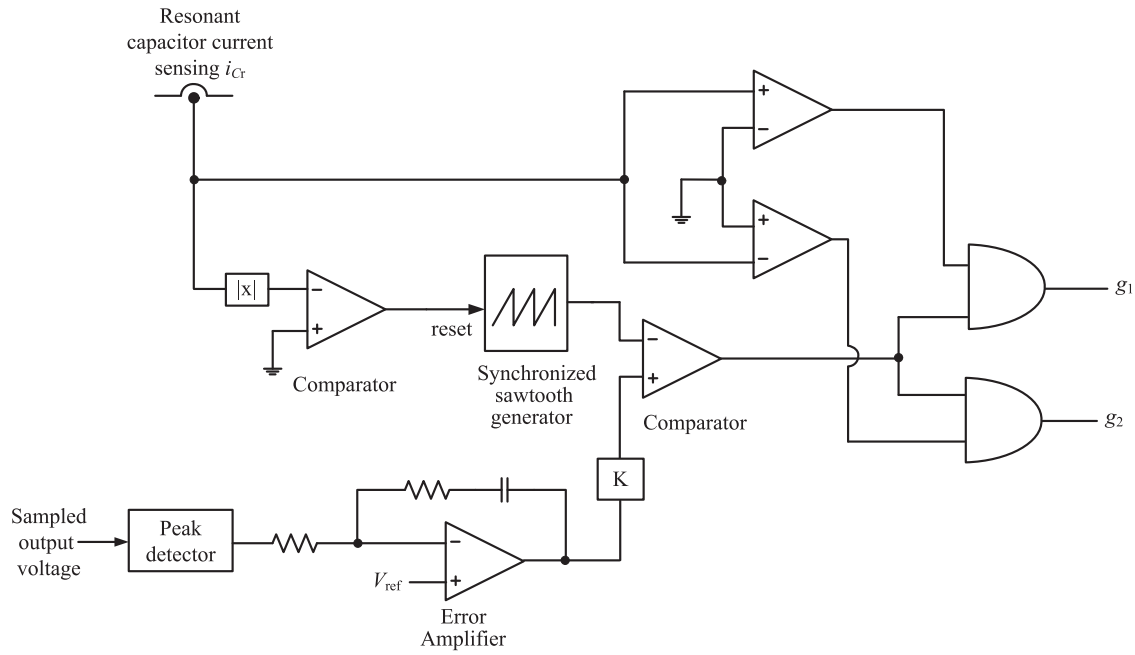

Fig. 14. Control block diagram of the SCC.

and is given by (13) as a function of α as plotted in Fig. 12 [21]

$$C_{\mathrm{eq}}(\alpha) = \frac{C_a}{2 - (2\alpha - \sin 2\alpha)/\pi} \tag{13}$$

where $\frac{\pi}{2} \leq \alpha < \pi$

C. Control of Constant-Frequency LCC Resonant Converter With SCC

In Fig. 13, it shows the complete schematic diagram of the proposed LCC resonant converter with the integration of SCC. The tunable capacitor is composed of an SCC and a series capacitor C_{s} which enables the modulation of f_{oc} by varying the

control angle of the SCC for providing output voltage regulation. The total equivalent resonant capacitance C_r is given by (14). The maximum value of C_r is equal to C_s when α is equal to π while the minimum value $C_s//C_a$ is attained when α is equal to $\pi/2$. In practice, an upper limit should be set for the maximum value of C_r to provide a sufficient range of variation of $f_{\rm oc}$ for the anticipated load failures. A reasonable value of α is 0.9π. The expression of the maximum and minimum value of C_r is given by (15) and (16), respectively. By solving (15) and (16) simultaneously, the required values of C_s and C_a can be determined and (17) gives the expression of C_s in terms of $C_{\rm r(max.)}$ and $C_{\rm r(min.)}$

$$C_r(\alpha) = \frac{C_s C_{\rm eq}}{C_s + C_{\rm eq}} = \frac{\pi C_s C_a}{\pi C_a + C_s\left(2\pi - 2\alpha + \sin 2\alpha\right)} \tag{14}$$

where $\frac{\pi}{2} \le \alpha < \pi$

$$C_{\rm r(max.)} = C_r(0.9\pi) \tag{15}$$

$$C_{\rm r(min.)} = \frac{C_s C_a}{C_s + C_a} \tag{16}$$

$$C_s = \frac{C_{\rm r(max.)} C_{\rm r(min.)}\left[\pi - 2\left(0.9\pi\right) + \sin\left(2\times 0.9\pi\right)\right]}{C_{\rm r(max.)}\left[2\pi - 2\left(0.9\pi\right) + \sin\left(2\times 0.9\pi\right)\right] - \pi C_{\rm r(min.)}} \tag{17}$$

$$C_a = \frac{C_{\rm r(min.)} C_s}{C_s - C_{\rm r(min.)}}. \tag{18}$$

As in typical resonant converters, the proposed resonant network is excited by a stepped-down bipolar square wave voltage source generated by a half-bridge circuit. To maintain the same common bus voltage v_o under any load conditions, the peak of v_o is sensed and regulated through feedback control. It is worthwhile to note that optocoupler or isolated sensing transformer is unnecessary for transmitting the sensed voltage signal to the primary-side of the proposed converter since all control procedure is done on the secondary side as a result of modulating the SCC. Fig. 14 depicts the control block diagram of the SCC. The sawtooth generator of the controller is synchronized with the sensed $i_{C\rm r}$ such that the sawtooth signal will be reset for every zero-crossing point of $i_{C\rm r}$. The required control angle α for the gate drive signal of S_1 or S_2 is generated by comparing the error voltage signal with the synchronized sawtooth signal. The generated gate drive signals will be subsequently applied to S_1 or S_2 according to the polarity of $i_{C\rm r}$, as explained in the previous section.

D. Design Procedure and Design Example

After identifying the desired operating point of the resonant network and conditions for achieving the desired operating range of SCC, a systematic design procedure and a design example based on the established design equations are presented in this section. It should be noted that the finished design (i.e., v_o, X_C) adopts the same specifications listed in Section II to enable a direct comparison with the experimental results presented in the next section.

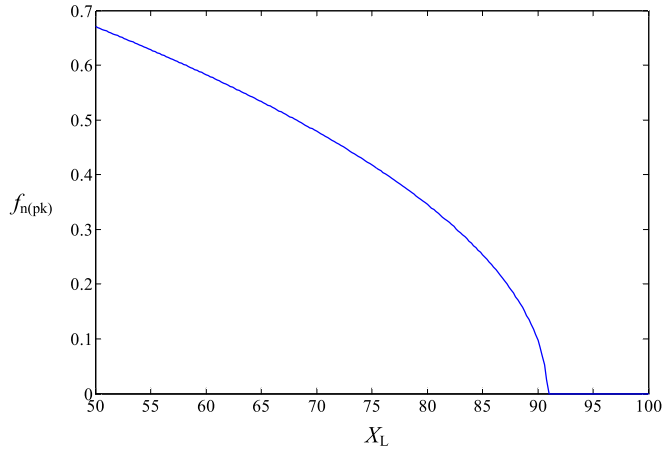

Fig. 15. Variation of $f_{n(\rm pk)}$ versus X_L.

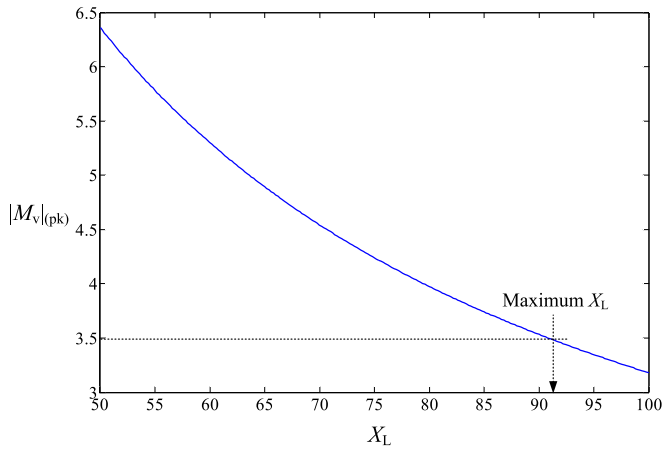

Fig. 16. Variation of peak voltage gain $|M_v|_{(\rm pk)}$ versus X_L.

Step 1: Choose a value of k in (4) such that the total load impedance is dominated by the balancing capacitor X_C and the current is mainly governed by X_C and remains insensitive to the variation of R_o. In our design, X_C is $84\ \Omega$ which is 3.5 times larger than R_o for meeting this requirement.

Step 2: Design the constant voltage gain of the resonant tank $|M_v|_{(\rm cvg)}$ for the nominal input voltage of the primary half-bridge circuit. Typically, the input voltage is supplied by a boost power-factor-correction preregulator (PFC). Therefore, the nominal input voltage of the half-bridge circuit $V_{\rm PFC}$ is set to 400 V while the required rms value of v_o is 168 V for delivering a total LED current of 2-$\rm A_{rms}$ ($400\ \rm mA_{rms} \times 5$) for 5 LED branches as determined by (3). Figs. 15 and 16 show the variation of $f_{n(\rm pk)}$ versus X_L and $|M_v|_{(\rm pk)}$ versus X_L, respectively, from which it can be seen that the solution of $f_{n(\rm pk)}$ reaches the minimum (i.e., $f_{n(\rm pk)} = 0$) beyond a certain value of X_L and $|M_v|_{(\rm pk)}$. Thus, the maximum value of X_L is restricted. In our design, $|M_v|_{(\rm cvg)}$ is chosen to be 2.05 and the corresponding X_L can be found by (9) which is equal to 82.

Step 3: After choosing the value of X_L for the nominal voltage gain requirement, the transformer's turns ratio N can be

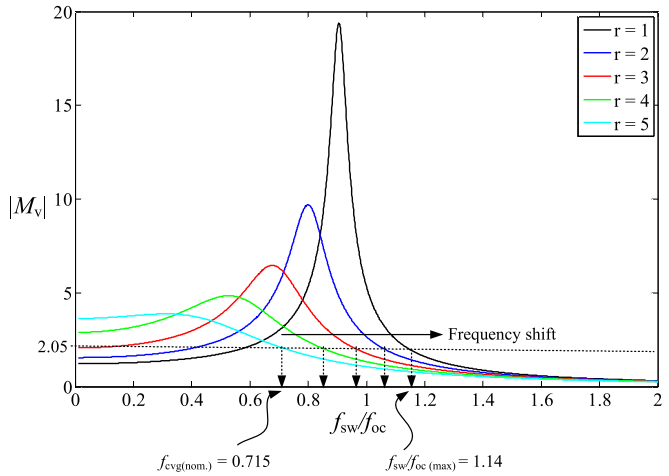

Fig. 17. Frequency responses of the SCC-based resonant network for different number of LED strings opened, where r is the number of conducting LED strings.

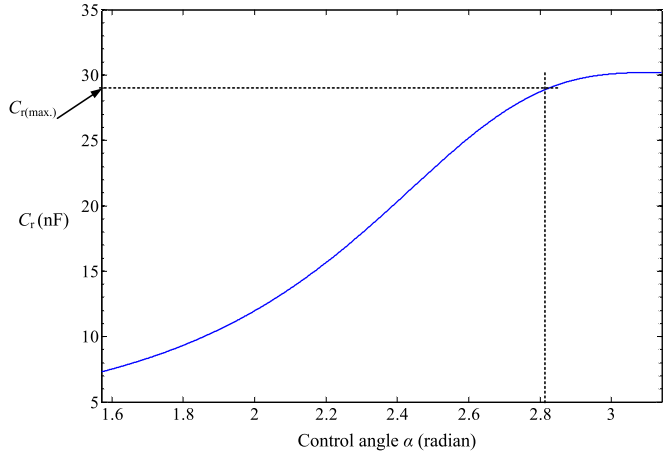

Fig. 18. Variation of equivalent resonant capacitance C_r with control angle α.

determined. The rms value of the fundamental component of the bipolar square wave is 82 V (i.e., 168 V/2.05). Hence, N can be found by (19) which is equal to 0.455

$$v_{\text{in}-f} = \frac{2\sqrt{2}}{\pi}\left(N \times \frac{1}{2}V_{\text{PFC}}\right) \tag{19}$$

where $v_{\text{in}-f}$ is the rms value of the fundamental component of the bipolar square wave and V_{PFC} is the input voltage supplied by the front-end PFC to the half-bridge circuit.

Step 4: Determine the required values of $C_{r(\max.)}$ and $C_{r(\min.)}$ for the minimum and maximum values of f_{oc}. Fig. 17 shows the resonant network's frequency responses for different number of opened LED strings, from which it can be found that the required ratio of $f_{\text{sw}}/f_{\text{oc}}$ is 1.14 for the worst case in which only one LED string is conducting. A switching frequency is chosen to solve for the value of f_{oc} and the corresponding C_r is obtained from (6). The switching frequency is chosen to be 87 kHz which is the same as the nominal frequency in Table I. The resonant inductance L_r is found to be 150 μH by using (7). Thus, $C_{r(\max.)}$ can be calculated as 29 nF. On the other hand, the value of $C_{r(\min.)}$ is found by the minimum input voltage condition (i.e., maximum voltage gain). The minimum V_{PFC} is set to be 280 V such that the required voltage gain is 2.9 and the corresponding $f_{\text{sw}}/f_{\text{oc}}$ is 0.571. As a result, the required $C_{r(\min.)}$ is 7.3 nF.

Step 5: Using (17) and (18) to determine the values of C_s and C_a, they are found to be 30.2 and 9.63 nF, respectively. The variation of C_r versus α is shown in Fig. 18. Finally, by substituting f_{sw} into (4), the total balancing capacitance C_o is found to be 21.7 nF while the individual balancing capacitance C_{bal} is 4.4 nF.

IV. Experimental Verification

In this section, a prototype of the designed LED driver is constructed and verified experimentally. The peak value of v_o is regulated at 240 V (i.e., $168\text{V}_{\text{rms}} \times \sqrt{2}$). The measured total LED current is 1.7 A_{rms} and the measured output power of the LED driver is 70 W. The actual component values used are listed in Table II. The AC-LED load is composed of a full-bridge rectifier and a smoothing capacitor. The number of LEDs per LED string is 15 such that the ac equivalent resistance of an LED string R_{LED} is 120 Ω.

TABLE II
List of Component Values

Transformer ratio N	62:28 = 0.452
C_{bal}	2.2 nF $\pm 5\% \times 2$
C_a	4.7 nF $\pm 5\% \times 2$
C_s	33 nF $\pm 10\%$
L_r	155 μH
Type of LEDs	Osram Opto LUW W5AM-KYLX-4E8G, 5700K $\times$ 15 per string
Half-bridge MOSFET	STP26NM60ND (21 A, 600 V)
SCC MOSFET	IRF 840 (8 A, 500 V)
Diode bridges	UF 5408 (3 A, 1000 V)

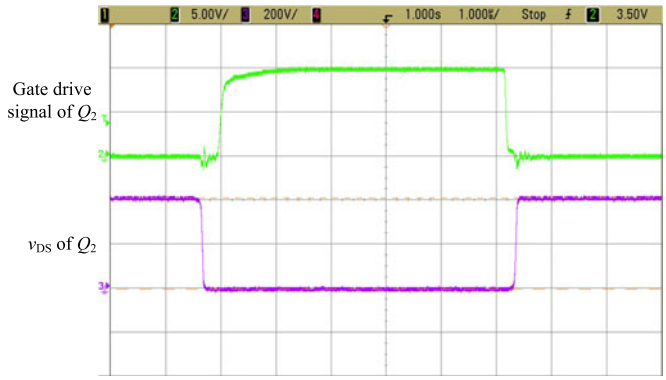

Fig. 19. Measured drain-to-source voltage waveform of Q_2 (200 V/DIV) and gate drive signal of Q_2 (5 V/DIV) under nominal condition.

Fig. 19 shows the measured waveforms of the gate drive signal of Q_2 and its drain-to-source voltage v_{DS} for the nominal case, where five LED strings are conducting. From Fig. 19, it can be seen that the v_{DS} of Q_2 falls to zero before the gate drive signal is applied, which means that ZVS is achieved, in agree-

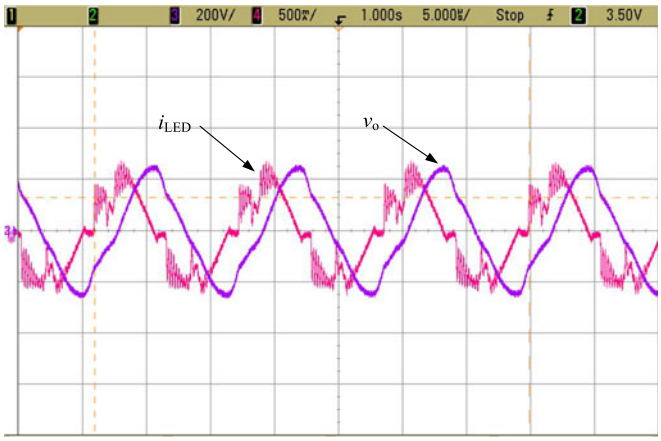

Fig. 20. Measured common bus voltage v_o (200 V/DIV) and LED current $i_{\rm LED}$ (500 mA/DIV) waveforms in String 5 under nominal condition.

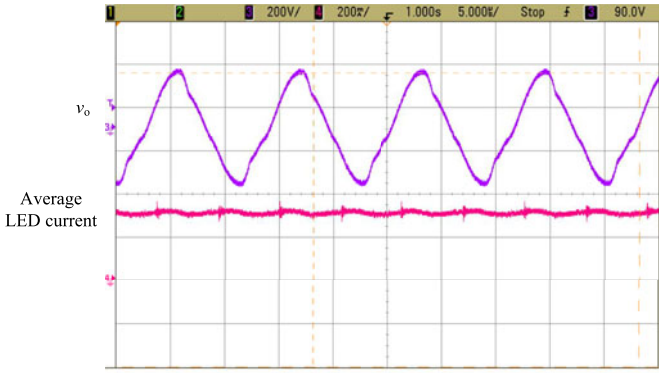

Fig. 21. Measured common bus voltage v_o (200 V/DIV) and average LED current (200 mA/DIV) waveforms after smoothing by capacitor in String 5 under nominal condition.

TABLE III
AVERAGE CURRENT IN DIFFERENT LED STRINGS IN NOMINAL CONDITION

String number n	5	4	3	2	1
Average LED current (mA)	312	312	316	314	311

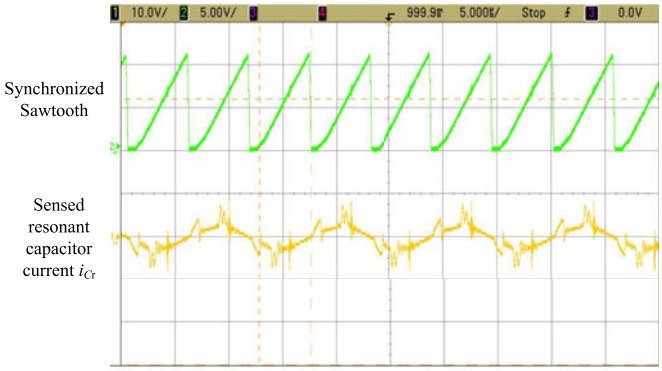

Fig. 22. Measured synchronized sawtooth (5 V/DIV) and sensed resonant capacitor current i_{Cr} (10 V/DIV) waveforms under nominal condition.

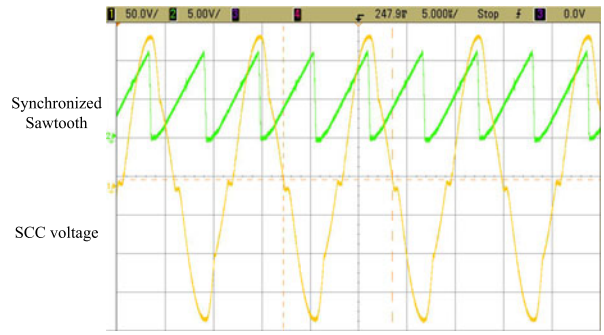

Fig. 23. Measured synchronized sawtooth (5 V/DIV) and SCC voltage (50 V/DIV) waveforms under nominal condition.

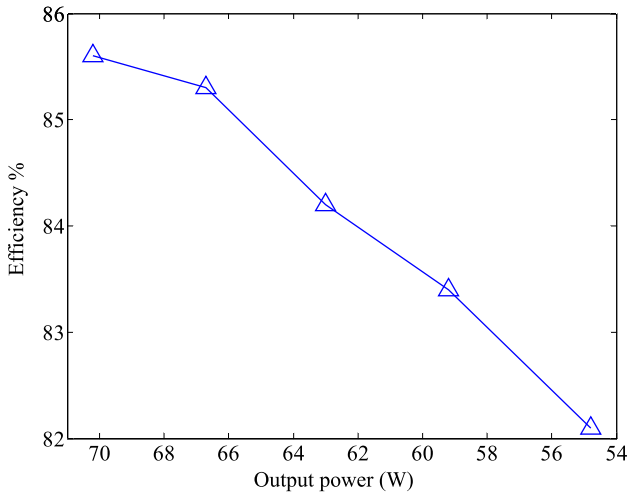

Fig. 24. Measured efficiency for different output power levels.

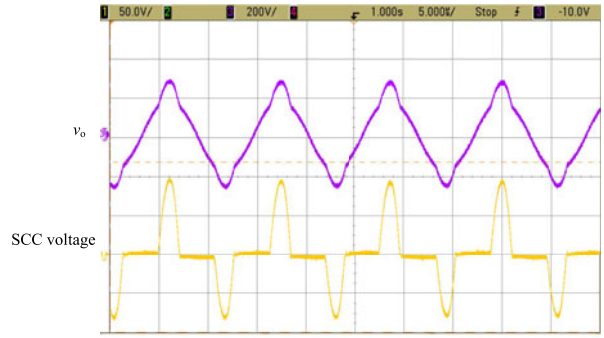

Fig. 25. Measured common bus voltage v_o (200 V/DIV) and SCC voltage (50 V/DIV) waveforms when only one string is conducting.

ment with the design objective. In addition, Fig. 20 shows the waveforms of the common bus voltage v_o and the branch LED current in String 5, from which it can be seen that $i_{\rm LED}$ leads v_o by 90°. Therefore, it confirms that the branch impedance is dominated by the balancing capacitive impedance. From the results of Figs. 19 and 20, the analysis in Section III-A is validated where ZVS can be automatically achieved by design as the operating point is located at $f_{\rm cvg(nom.)}$ and the condition $X_C >> R_o$ is satisfied for current balancing.

Fig. 21 shows the waveforms of the common bus voltage v_o and the average LED current in String 5. The latter is smoothed

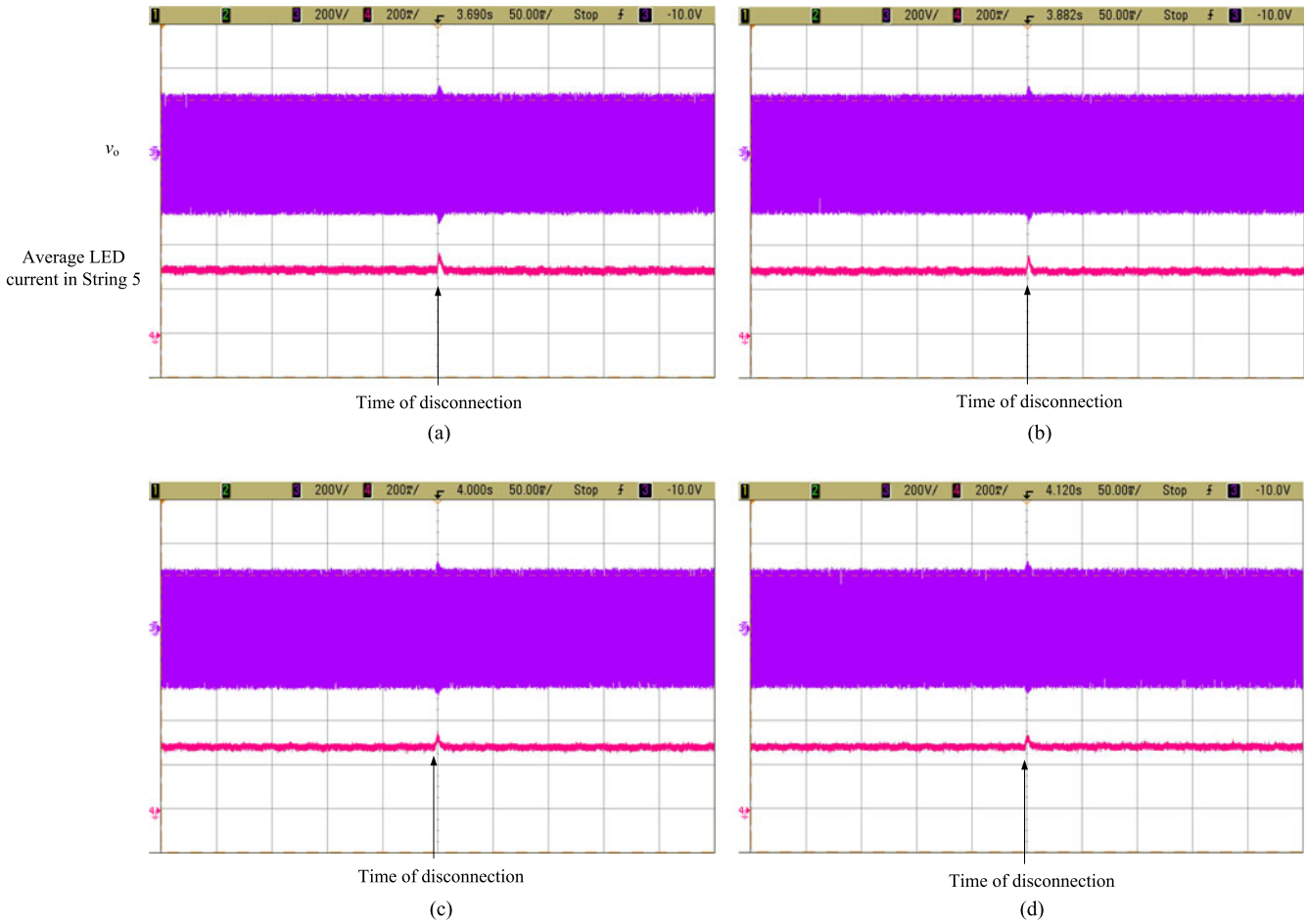

Fig. 26. Measured transient common bus voltage v_o (200 V/DIV) and average LED current (200 mA/DIV) waveforms in String 5 when other LED strings are opened one after another, (a) String 4 opened, (b) String 3 opened, (c) String 2 opened, and (d) String 1 opened.

by a 2.2 μF capacitor which is connected in parallel with the LED string. The average LED current after smoothing by capacitor is 312 mA. Table III shows the average current in different LED strings from which it can be seen that the average current varies from 311 to 316 mA. The maximum current deviation under nominal condition is calculated as 1.61%.

Fig. 22 shows the waveforms of the synchronized sawtooth and the resonant capacitor current i_{Cr} sensed by current transformer under nominal condition. It can be seen that the sawtooth signal is reset at the zero-crossing points of i_{Cr} such that either S_1 or S_2 is turned on depending on the polarity of i_{Cr}. Fig. 23 shows the SCC voltage waveform under nominal condition and Fig. 24 plots the measured efficiency for different output power levels with different R_o. It shows that the driver's efficiency decreases with R_o due to the increased conduction loss, which agrees with the analysis in Section III-A. The driver's efficiency can be improved by optimizing the magnetic design and component values.

Finally, in order to study the effectiveness of isolating the failed LED strings from the working LED strings, the prototype is subjected to disconnection tests where LED strings are switched opened. Fig. 25 shows the SCC voltage waveform for only one conducting string. It shows that the waveform has longer dead time and smaller voltage amplitude compared with Fig. 23 because of larger α for the regulation of v_o. Fig. 26(a) to (d) shows the transient waveforms of the common bus voltage v_o and the average LED current in String 5 when other LED strings are opened one after another, from which it can be seen that the current in the working LED string can be maintained approximately constant as a result of the tightly regulated v_o and constant balancing capacitive impedance. Table IV calculates the average current variation in String 5 after other LED strings are opened. The maximum variation is -2.56% which is significantly lower than +34% predicted by the simulation results in Section II.

TABLE IV
AVERAGE CURRENT IN STRING 5 AFTER OTHER LED STRINGS ARE OPENED

Conducting Strings	Average current in String 5 (mA)	% Variation
5	312	/
4	308	-1.28%
3	307	-1.60%
2	305	-2.24%
1	304	-2.56%

V. Conclusion

This paper proposes a constant-frequency capacitive current balancing method for parallel-connected LED strings. In contrast to conventional regulation method, output voltage regulation of the resonant converter is accomplished by modulating the resonant frequency of the resonant network. Consequently, the common ac bus voltage and the impedance of the balancing capacitors can be kept constant over a wide range of load conditions, and hence continuous and constant-current operation are guaranteed in the working LED strings when other strings are malfunctioning. The existing LCC resonant network is used as a case study to illustrate the problem inherent with conventional regulation method and its failure to provide tight current regulation in LED strings when load failures occur. The technique of SCC is discussed and adopted in the existing LCC resonant converter to realize the proposed method. A systematic design procedure is presented and a 70-W experimental prototype is constructed for verification. The experimental results demonstrate that the currents in the working LED strings are tightly regulated and maintained before and after other LED strings are opened. Despite that the present study emphasizes on LCC resonant network, the general idea can be further extended to other types of resonant networks to harvest the same performance benefits.

References

[1] A. Zukauskas, M. S. Shur, and R. Gaska, *Introduction to Solid-State Lighting*. Hoboken, NJ, USA: Wiley, 2002.

[2] S. Choi and T. Kim, "Symmetric current-balancing circuit for LED backlight with dimming," *IEEE Trans. Ind. Electron.*, vol. 59, no. 4, pp. 1698–1707, Apr. 2012.

[3] X. Qu, S.-C. Wong, and C. K. Tse, "A current balancing scheme with high luminous efficacy for high-power LED lighting," *IEEE Trans. Power Electron.*, vol. 29, no. 6, pp. 2649–2654, Jun. 2014.

[4] H.-J. Chiu, Y.-K. Lo, J.-T. Chen, S.-J. Cheng, C.-Y. Lin, and S.-C. Mou, "A high-efficiency dimmable LED driver for low-power lighting applications," *IEEE Trans. Ind. Electron.*, vol. 57, no. 2, pp. 735–743, Feb. 2010.

[5] Y. Hu and M. Jovanovic, "LED driver with self-adaptive drive voltage," *IEEE Trans. Power Electron.*, vol. 23, no. 6, pp. 3116–3125, Nov. 2008.

[6] C.-L. Chiu and K.-H. Chen, "A high accuracy current-balanced control technique for LED backlight," in *Proc. IEEE Power Electron. Spec. Conf.*, Jun. 2008, pp. 4202–4206.

[7] S. N. Li, W. Zhong, W. Chen, and S. Hui, "Novel self-configurable current-mirror techniques for reducing current imbalance in parallel light-emitting diode (LED) strings," *IEEE Trans. Power Electron.*, vol. 27, no. 4, pp. 2153–2162, 2012.

[8] H.-J. Chiu and S.-J. Cheng, "LED backlight driving system for large-scale LCD panels," *IEEE Trans. Ind. Electron.*, vol. 54, no. 5, pp. 2751–2760, Oct. 2007.

[9] Y. Hu and M. Jovanovic, "A new current-balancing method for paralleled LED strings," in *Proc. IEEE 26th Annu. Appl. Power Electron. Conf. Expo.*, Mar. 2011, pp. 705–712.

[10] K.-H. Jung, J.-W. Yoo, and C.-Y. Park, "A design of current balancing circuit for parallel connected LED strings using balancing transformers," in *Proc. IEEE 8th Int. Conf. Power Electron. ECCE Asia*, May. 2011, pp. 528–535.

[11] X. Wu, Z. Wang, and J. Zhang, "Design considerations for dual-output quasi-resonant flyback LED driver with current-sharing transformer," *IEEE Trans. Power Electron.*, vol. 28, no. 10, pp. 4820–4830, Oct. 2013.

[12] H. Wu, S. Ji, F. Lee, and X. Wu, "Multi-channel constant current (MC3) LLC resonant LED driver," in *Proc. IEEE Energy Convers. Congr. Expo.*, Sep. 2011, pp. 2568–2575.

[13] S. Baddela and D. Zinger, "Parallel connected LEDs operated at high frequency to improve current sharing," in *Proc. IEEE 39th IAS Annu. Meeting Ind. Appl. Conf.*, vol. 3, Oct. 2004, pp. 1677–1681.

[14] K. H. Loo, Y. M. Lai, and C. K. Tse, "Design and analysis of LCC resonant network for quasi-lossless current balancing in multistring AC-LED srray," *IEEE Trans. Power Electron.*, vol. 28, no. 2, pp. 1047–1059, Feb. 2013.

[15] X. Wu, J. Zhang, and Z. Qian, "A simple two-channel LED driver with automatic precise current sharing," *IEEE Trans. Ind. Electron.*, vol. 58, no. 10, pp. 4783–4788, Oct. 2011.

[16] X. Qu, S.-C. Wong, and C. Tse, "An improved LCLC current-source-output multistring LED driver with capacitive current balancing," *IEEE Trans. Power Electron.*, vol. 30, no. 10, pp. 5783–5791, Oct. 2015.

[17] R. Zhang and H. S.-H. Chung, "Capacitor-isolated multistring LED driver with daisy-chained transformers," *IEEE Trans. Power Electron.*, vol. 30, no. 7, pp. 3860–3875, Jul. 2015.

[18] C. Zhao, X. Xie, and S. Liu, "Multioutput LED drivers with precise Passive current balancing," *IEEE Trans. Power Electron.*, vol. 28, no. 3, pp. 1438–1448, Mar. 2013.

[19] X. Wu, C. Hu, J. Zhang, and Z. Qian, "Analysis and design considerations of LLCC resonant multioutput DC/DC LED driver with charge balancing and exchanging of secondary series resonant capacitors," *IEEE Trans. Power Electron.*, vol. 30, no. 2, pp. 780–789, Feb. 2015.

[20] J. Zhang, J. Wang, and X. Wu, "A capacitor-isolated LED driver with inherent current balance capability," *IEEE Trans. Ind. Electron.*, vol. 59, no. 4, pp. 1708–1716, Apr. 2012.

[21] W.-J. Gu and K. Harada, "A new method to regulate resonant converters," *IEEE Trans. Power Electron.*, vol. 3, no. 4, pp. 430–439, Oct. 1988.

[22] Z. Hu, Y. Qiu, L. Wang, and Y.-F. Liu, "An interleaved LLC resonant converter operating at constant switching frequency," *IEEE Trans. Power Electron.*, vol. 29, no. 6, pp. 2931–2943, Jun. 2014.

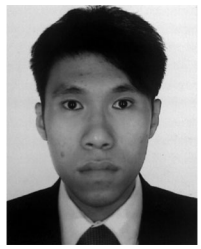

C. S. Wong (S'14) received the B.Eng. (Hons.) degree in electronic and information engineering from The Hong Kong Polytechnic University, Kowloon, Hong Kong, in 2013, where he is currently working toward the Ph.D. degree.

His research interests include LED driver circuit design and power-factor-correction regulators.

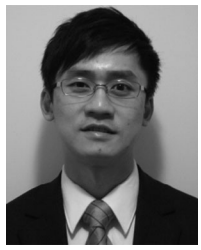

K. H. Loo (S'97–M'99) received the B.Eng. (Hons.) in electronic engineering and the Ph.D. degree from the University of Sheffield, U.K., in 1999 and 2002, respectively.

From 2002 to 2004, he was the Postdoctoral Fellow at Japan Society for the Promotion of Science, Ehime University, Matsuyama, Japan. In 2006, he joined the Hong Kong Polytechnic University as an Instructor in the Faculty of Engineering. He is currently an Assistant Professor in the Department of Electronic and Information Engineering, Hong Kong Polytechnic University, Hung Hom, Hong Kong. His research interests include power electronics for LED lighting and renewable energy systems.

Dr. Loo has been an Associate Editor for the IEEE Transactions on Energy Conversion since 2013.

Y. M. Lai (M'92–SM'11) received the B.Eng. degree in electrical engineering from the University of Western Australia, Perth, Australia, the M.Eng.Sc. degree in electrical engineering from the University of Sydney, Sydney, Australia, and the Ph.D. degree from Brunel University, London, U.K., in 1983, 1986, and 1997, respectively.

He is currently an Associate Professor with Hong Kong Polytechnic University, Hung Hom, Hong Kong, and his research interests include computer-aided design of power electronics and non-linear dynamics.

Martin H. L. Chow (M'98) received the B.Sc. degree in electrical engineering from the University of Hong Kong, Pok Fu Lam, Hong Kong, the M.Sc. degree in systems engineering from the University of Surrey, Guildford, U.K., and the Ph.D. degree in the area of power-factor-corrected switching regulators from The Hong Kong Polytechnic University, Hung Hom, Hong Kong, in 1980, 1984, and 1999, respectively.

In the course of his career, he has worked in shortwave radio circuit design with Philips, Hong Kong and in switch-mode power supplies design with Thomson, Singapore. In 1985, he started his teaching career at The Hong Kong Polytechnic University and is currently a Senior Lecturer in the Department of Electronic and Information Engineering.

Dr. Chow received the IEEE Power Electronics Society Transactions Prize Paper Award in 2001.

Chi K. Tse (M'90–SM'97–F'06) received the B.Eng. (Hons.) degree in electrical engineering and the Ph.D. degree from the University of Melbourne, Melbourne, Australia, in 1987 and 1991, respectively.

From 2005 to 2012, he was the Head of the Department of Electronic and Information Engineering, Hong Kong Polytechnic University, Hong Kong, where he is currently the Chair Professor . He is the author/co-author of 10 books, 20 book chapters, and more than 500 papers in research journals and conference proceedings, and holds 5 US patents.

Dr. Tse received the Best Paper Award by the IEEE TRANSACTIONS ON POWER ELECTRONICS in 2001, the Best Paper Award by *International Journal of Circuit Theory and Applications* in 2003, two Gold Medals at the International Inventions Exhibition in Geneva in 2009 and 2013, and a number of recognitions by the academic and research communities, including honorary professorship by several Chinese and Australian Universities, Chang Jiang Scholar Chair Professorship, IEEE Distinguished Lectureship, Distinguished Research Fellowship by the University of Calgary, Gledden Fellowship and International Distinguished Professorship-at-Large by the University of Western Australia. While with the Hong Kong Polytechnic University, he received the President's Award for Outstanding Research Performance twice, Faculty Research Grant Achievement Award twice, Faculty Best Researcher Award, and several teaching awards. He serves and has served as the Editor-in-Chief for the IEEE TRANSACTIONS ON CIRCUITS AND SYSTEMS II (2016–2017), the IEEE CIRCUITS AND SYSTEMS MAGAZINE (2012–2015), the IEEE CIRCUITS AND SYSTEMS SOCIETY NEWSLETTER (since 2007), an Associate Editor for three IEEE Journal/Transactions, Editor for *International Journal of Circuit Theory and Applications*, and is on the editorial boards of a few other journals. He also serves as a panel member of Hong Kong Research Grants Council and NSFC, and a member of several professional and government committees.